Electron-paramagnetic-resonance identification of transition-metal (Cr,Fe)–shallow-impurity (S,Zn) pairs in GaP

J. Kreissl
Forschungsstelle für Kristallzüchtung, Rudower Chaussee 6, D/O-1199 Berlin, Federal Republic of Germany

W. Ulrici
Paul-Drude-Institut für Festkörperelektronik, Hausvogteiplatz 5/7, D/O-1086 Berlin, Federal Republic of Germany

U. Rehse and W. Gehlhoff
Forschungsstelle für Kristallzüchtung, Rudower Chaussee 6, D/O-1199 Berlin, Federal Republic of Germany
(Received 12 July 1991)

Three Fe- or Cr-related EPR spectra are observed in liquid-encapsulated-Czochralski-grown GaP. The spectra in *n*-type GaP:Fe:S and GaP:Cr:S show trigonal symmetry. Their analysis suggests that the spectra are caused by the donor-acceptor nearest-neighbor pair defects [Fe_{Ga}^{+}-S_P] and [Cr_{Ga}^{+}-S_P]. In *p*-type GaP:Cr:Zn the spectrum reveals a Cr center of monoclinic symmetry. This center is identified as a [Cr_{Ga}^{3+}-Zn_{Ga}] pair. The concentration of the three pair defects shows that Coulomb attraction is responsible for the donor-acceptor pair formation.

I. INTRODUCTION

Transition-metal (TM) defects in III-V semiconductors have gained considerable interest during the past decade, when most of the activities were focused on isolated TM's of the first-row elements (electronic configuration $3d^n$). The currently accepted model of these defects suggests that the TM atoms are located on III sites (e.g., T_{Ga} in GaAs and GaP, where T denotes the transition metal) and act as more or less deep acceptors (single or double acceptors). However, some of them (Ti, V, Cr) have been found acting also as deep donors.[1,2] This different behavior depends on the position of the Fermi level determined by other dopants or residual impurities.

Comparatively less information is established about complexes or associates of TM's with other impurities or intrinsic defects in as-grown material. The largest group are the pair defects consisting of the double acceptor Ni_{Ga}^{+} and shallow donors (S, Se, or Te on V sites and Si, Ge, or Sn on III sites). These Ni_{Ga}^{+} pair defects have been identified in GaAs and GaP by optical absorption and photoluminescence due to the internal $^2T_2 \leftrightarrow {}^2E$ transitions of Ni^{+}.[3] In the case of GaP:Ni:S, uniaxial stress experiments revealed the trigonal symmetry of the Ni_{Ga}^{+}-S_P center supporting the nearest-neighbor model of this kind of pair. The first unequivocally identified pair defect of trigonal symmetry was the Mn_{Ga}^{2+}-S_P pair in GaP detected by EPR.[4] A Co_{Ga}^{2+}-Te_{As} complex in GaAs was found by photoluminescence, optical absorption, and EPR experiments.[5] Much effort has been devoted to the Cr_{Ga}^{2+} center of trigonal symmetry in GaAs responsible for the sharp lines around 0.839 eV due to the $^5T_2 \leftrightarrow {}^5E$ transitions of Cr^{2+} measured by photoluminescence and optical absorption (see Ref. 1 for a review). Now it is generally accepted that this center consists of Cr_{Ga}^{2+} associated with a nearest-neighbor arsenic vacancy. This interpretation is supported by the analysis of analogous spectroscopic features found in GaAs:Cr:Te and assigned to a Cr_{Ga}^{2+}-Te_{As} complex.[6,7] Centers of Cu_{Ga} complexed with interstitial defects (e.g., Li_i,C_i; see Refs. 8, 9, and references therein) were detected by optically detected magnetic resonance (ODMR) experiments on the triplet bound-exciton states of these centers. Complex centers of Mn_{Ga}^{2+} associated with interstitial Li having orthorhombic symmetry were investigated in GaAs and GaP by EPR.[10]

In all complexes identified so far the transition-metal impurity acts as a deep acceptor which is associated with a shallow donor. Contrary to this, no center was found until now with the T_{Ga} acting as a deep donor ($Ti_{Ga}^{3+}/Ti_{Ga}^{4+}$ level) forming a complex with a shallow acceptor. On the other hand, in silicon complexes a transition-metal donor and a shallow acceptor are well investigated (e.g., Ref. 11). However, it has to be noted that in contrast to the III-V semiconductors, in silicon the TM's in the pairs are located on interstitial sites.

Therefore we have searched for donor-acceptor pairs in liquid-encapsulated-Czochralski (LEC) grown GaP doped with the transition metal Cr or Fe and codoped in each case with the shallow donor S or with the shallow acceptor Zn. For GaP:Cr:S, GaP:Fe:S, and GaP:Cr:Zn we have observed angular-dependent EPR spectra. In this paper we will analyze these EPR spectra and attribute them to Cr-S and Fe-S pairs of trigonal symmetry and Cr-Zn pairs of monoclinic symmetry. With the Cr-Zn pair a donor-acceptor pair is identified in III-V semiconductors in which the T_{Ga} acts as a deep donor. A preliminary report on our studies of the Cr-related pairs was presented recently.[12]

II. EXPERIMENT

The oriented samples were prepared from the tail end of LEC-grown GaP boules (diameter 40 mm, length

about 100 mm) codoped with Cr or Fe and S or Zn in the melt. The contents determined by spectrochemical analysis at the tail end of GaP:Cr:S are [Cr]=1.7×10^{17} cm^3, and [S]=6.7×10^{17} cm^{-3}, and those of GaP:Cr:Zn are [Cr]=3.0×10^{17} cm^{-3} and [Zn]=4.8×10^{17} cm^{-3}. The contents of the tail end samples of Fe-doped boules are for GaP:Fe:S [Fe]=5×10^{17} cm^{-3},[S]=4×10^{17} cm^{-3} and GaP:Fe:Zn[Fe]=2×10^{17} cm^{-3},[Zn]=5×10^{17} cm^{-3}. The EPR measurements were performed in the X band using a ZWG 230 spectrometer equipped with a fixed temperature cryostat ($T=20.4$ K) and a He gas-flow cryostat (Oxford ESR 900) for measurements at variable temperature. The magnetic field was rotated in a {110} plane of the crystal.

III. RESULTS

A. GaP:Fe:S and GaP:Cr:S

In n-type GaP samples codoped with S and Fe the well-known EPR signal of the isolated double-acceptor defect $Fe_{Ga}^{+}(A^{2-})$ is observed (linewidth $\Delta B_{pp}=2.8$ mT).[13] Here, in general, the designation for the center is showing the oxidation state of the T_{Ga} (as determined by EPR) as well as the net charge of the impurity A in the semiconductor. In addition to this intense signal, an angular-dependent EPR spectrum with considerably smaller intensity was measured. The spectra are shown for the three main directions (**B**$\|\langle 110\rangle$, $\langle 111\rangle$, and $\langle 100\rangle$) in Fig. 1. The iron doping and the linewidth ΔB_{pp} of about 3 mT which is comparable with the linewidth of the $Fe_{Ga}^{+}(A^{2-})$ spectrum makes it highly probable that this spectrum can be assigned to an iron-related defect. The measured angular dependence [besides the weakly angular-dependent signal of $Fe_{Ga}^{+}(A^{2-})$] is plotted as solid circles in Fig. 2(b). The general feature of this angular dependence with a maximum at **B**$\|\langle 111\rangle$ shows the behavior of a defect with trigonal symmetry. We will prove by our analysis that we have observed a spectrum caused by $Fe_{Ga}^{+}(A^{2-})$ with a $3d^7$ electronic configuration in a strong trigonal distorted cubic crystal field. The origin of the trigonal crystal-field distortion should be a further lattice defect where a closed-shell $S_P^{6+}(A^{+})$ ion substitutional on a P site is most probable. Therefore the defect is named [$Fe_{Ga}^{+}(A^{2-})$-$S_P^{6+}(A^{+})$] (see Sec. IV).

The ground state of Fe_{Ga}^{+} is the orbital singlet $^4A_2$. The energy levels of such a system can be described by the spin Hamiltonian with $S=\frac{3}{2}$,

$$\mathcal{H}=g_{\|}\mu_B B_z S_z+g_{\perp}\mu_B(B_x S_x+B_y S_y)+D[S_z^2-\tfrac{1}{3}S(S+1)]. \quad (1)$$

All symbols have their usual meanings. The z axis of the coordinate system (x,y,z) coincides with the trigonal C_3 symmetry axis parallel to $\langle 111\rangle$. The x and y axes in (1) are arbitrary in the plane perpendicular to z. Including higher-order terms in (1) which requires a decision like in the case of the Cr^{+}-related pair discussed below, the x and y axes are chosen parallel to $[\bar{1}\,\bar{1}2]$ and $[1\bar{1}0]$ for z parallel to [111]. According to the four C_3 directions there are four different center positions, two of which are

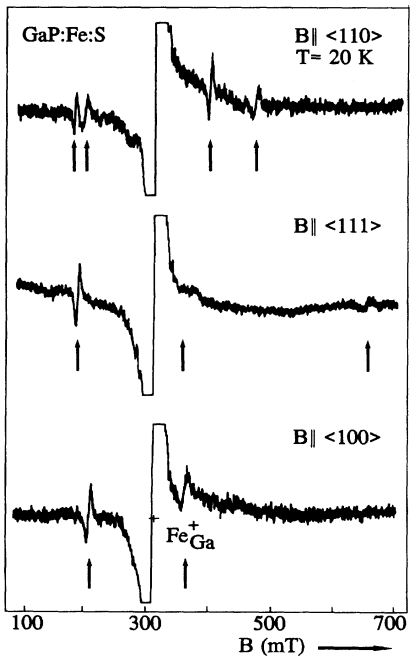

FIG. 1. EPR spectra of GaP:Fe:S for the three main directions. The transitions belonging to the trigonal [$Fe_{Ga}^{+}(A^{2-})$-$S_P^{6+}(A^{+})$] pair are marked by arrows. The intense signal is due to the isolated double acceptor $Fe_{Ga}^{+}(A^{2-})$. The measurements were performed at $T=20$ K with the microwave frequency of 9.221 GHz.

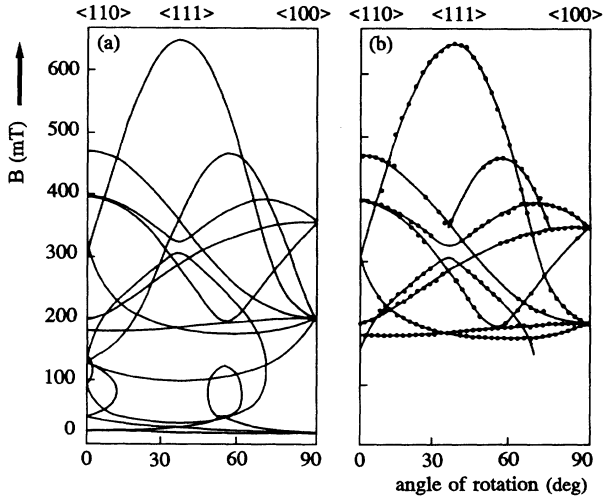

FIG. 2. Angular dependence of the fine-structure line positions of the [$Fe_{Ga}^{+}(A^{2-})$-$S_P^{6+}(A^{+})$] pair obtained at 9.221 GHz. The magnetic field is rotated in a {110} plane. (a) A plot of all possible fine-structure transitions. The parameters of the calculation are given in Table I. (b) The experimental data are plotted as solid circles. Those parts of the calculated angular dependence for which experimental data exist are shown as solid lines.

always magnetically equivalent under rotation around a ⟨110⟩ axis as it was done in our experiments. The estimation of the zero-field splitting parameter D for the ⟨111⟩ direction shows that the trigonal zero-field splitting and the Zeeman splitting are very similar in the magnetic-field range where the EPR transitions occur (intermediate case). Since for arbitrary directions perturbation theory cannot be used for the solution of the energy matrix of the spin Hamiltonian (1) in a truly intermediate case, we have applied the method of direct diagonalization of the $S=\frac{3}{2}$ energy matrix. Using a computer procedure for the calculation of line positions and intensities via the calculation of eigenvalues and eigenfunctions for the Hamiltonian (1), a good agreement between the measured and calculated line positions and intensities could be obtained for the angular dependence of all observed fine-structure transitions. The results of the theoretical calculations are shown in Fig. 2. In Fig. 2(a) all possible EPR transitions are included as solid lines. In Fig. 2(b) the calculated curves for which experimental data exist are included as solid lines in order to show the good agreement between theory and experiment. The parameters $g_{\parallel}$, $g_{\perp}$, and D resulting from the best fit of the experimental points are given in Table I.

In Fig. 3 the energy-level structure of the $^4A_2$ ground-state multiplet is plotted as a function of the magnetic field for the magnetic field oriented (a) parallel and (b) perpendicular to the trigonal C_3 axis. The calculation was done assuming a negative sign of D. The sign of the zero-field parameter D determines the sequence of the energy levels at zero magnetic field, but does not influence the EPR line positions in this case. The sign can be determined from a comparison of the EPR intensities with the theoretical transition probabilities, including the effect of Boltzmann population of the energy levels for different temperatures. The temperature dependence of the intensities of the transitions at $B=177$ and 466 mT for $\mathbf{B}\parallel\langle 110\rangle$ led us conclude that D is negative. In the parallel case there is no mixing of states. Therefore only "allowed" electronic spin transitions with $\Delta M=\pm 1$ could be observed [these transitions are indicated by bold arrows in Fig. 3(a)]. For arbitrary directions a strong mixture of states occurs. This can be seen in Fig. 3(b) for the perpendicular case, where neither the high-magnetic-field quantum numbers nor the quantum numbers defined by the trigonal crystal field are good quantum numbers in the magnetic-field range in which the EPR transitions occur.

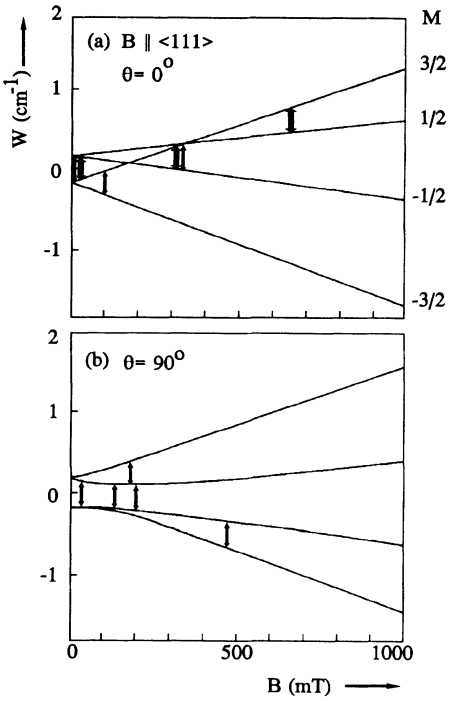

FIG. 3. Energy-level diagram for the $[Fe_{Ga}^{+}(A^{2-})\text{-}S_P^{6+}(A^{+})]$ defect for the magnetic field oriented parallel (a) and perpendicular (b) to the trigonal pair axis. EPR transitions at 9.221 GHz are indicated. For an exact parallel orientation (a) only allowed $\Delta M=\pm 1$ electronic spin transitions have a transition probability not equal to zero (bold arrows).

The assignment of the spectrum to a Fe_{Ga}^{+}-related defect is additionally supported by the observed g values

TABLE I. Data for three types of pair defects in GaP.

Defect	Spin	Symmetry and axes	g values	Zero-field splitting parameters (cm^{-1})
$[Fe_{Ga}^{+}(A^{2-})\text{-}S_P^{6+}(A^{+})]$	$\frac{3}{2}$	trigonal $\mathbf{z}\parallel\langle 111\rangle$	$g_{\parallel}=2.133(5)$ $g_{\perp}=2.140(5)$	$D=-0.1705(3)$
$[Cr_{Ga}^{+}(A^{2-})\text{-}S_P^{6+}(A^{+})]$	$\frac{5}{2}$	trigonal $\mathbf{z}\parallel\langle 111\rangle$ $\mathbf{x}\parallel\langle 112\rangle$ $\mathbf{y}\parallel\langle 110\rangle$	$g_{\parallel}=2.000(5)$ $g_{\perp}=g_{\parallel}$	$\lvert D\rvert=0.0091(1)$ a,F not determined (see text)
$[Cr_{Ga}^{3+}(A^{0})\text{-}Zn_{Ga}^{2+}(A^{-})]$	$\frac{3}{2}$	monoclinic $\mathbf{z}\parallel\langle 110\rangle$ $\mathbf{x}\parallel\langle 110\rangle$ $\mathbf{y}\parallel\langle 100\rangle$	$g_{xx}=g_{yy}=g_{zz}=2.000(5)$ $g_{xy}=g_{xz}=g_{yz}\leq 10^{-3}$	$D_{zz}=-0.102(3)$ $D_{xx}=0.098(3)$ $D_{yy}=0.004(3)$ $D_{yz}=0.020(3)$ $D_{xz}=D_{xy}=0$

(see Table I). The g values show the typical shift for $3d^7$ ions in a tetrahedral crystal field. According to the relation $g=g_e-8k\lambda_0/\Delta$ we get a reasonable value $k=0.7$ for the covalency reduction factor if we use the free-ion spin-orbit coupling constant of Fe^+ $\lambda_0=-119$ cm^{-1} (Ref. 14) and the $^4A_2$-$^4T_2$ distance $\Delta=5080$ cm^{-1} from the $\sigma_n^0(h\nu)$ spectrum obtained by optical deep-level transient spectroscopy (DLTS).[15] The concentration of the $[Fe_{Ga}^+(A^{2-})$-$S_P^{6+}(A^+)]$ pair was estimated to be about 3% of the isolated $Fe_{Ga}^+(A^{2-})$ center.

In the n-type GaP samples codoped with S and Cr the well-known EPR spectrum of the isolated $Cr_{Ga}^+(A^{2-})$ defect[16] was measured with a large intensity (linewidth $\Delta B_{pp}=13$ mT) as well as that of the isolated $Fe_{Ga}^+(A^{2-})$ due to residual iron. Additionally, a weaker spectrum was observed which is marked by arrows in Fig. 4. The angular dependence of this spectrum is plotted as bold circles in Fig. 5. Because of the superposition of the angular dependent spectrum with the very intense one of isolated $Cr_{Ga}^+(A^{2-})$, only those transitions occurring outside the magnetic-field range of the isolated Cr_{Ga}^+ signal are detectable. From the behavior of the angular dependences shown in Fig. 5 with the characteristic maximum at $\mathbf{B}\|\langle 111\rangle$, it follows that the observed defect has trigonal symmetry. The linewidth ΔB_{pp} of the spectrum which is of the same magnitude as ΔB_{pp} of the isolated Cr_{Ga}^+ defect and the fact that we observe this spectrum only in n-type GaP codoped with Cr and S suggests a pair defect consisting of a Cr_{Ga}^+ ion with a $^6S_{5/2}$ ground state in a trigonal distorted cubic crystal field. As in the case of the $[Fe_{Ga}^+(A^{2-})$-$S_P^{6+}(A^+)]$ pair, an associated closed-shell $S_P^{6+}(A^+)$ ion on a nearest-neighbor phosphorus site should be the reason for the trigonal distortion (see Sec. IV). The defect is called $[Cr_{Ga}^+(A^{2-})$-$S_P^{6+}(A^+)]$.

The spin Hamiltonian (1) extended by the terms proportional to S^4 (parameters a and F) can be used for the description of the EPR spectrum within the $^6S_{5/2}$ ground-state multiplet of a $3d^5$ chromium ion (cf. Ref. 14). The tensor axes and the number of center positions have already been discussed after Eq. (1) for the similar

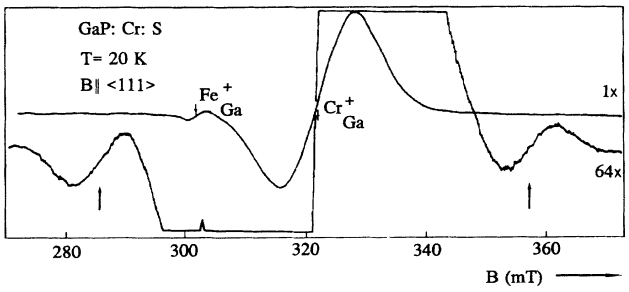

FIG. 4. EPR spectrum of GaP:Cr:S measured at $T=20$ K with the microwave frequency of 9.01 GHz for the orientation $\mathbf{B}\|\langle 111\rangle$. The upper spectrum with a lower receiver gain (1×) shows the dominating isolated defect, $Cr_{Ga}^+(A^{2-})$, and the line of $Fe_{Ga}^+(A^{2-})$ due to residual iron. In the lower spectrum with the higher receiver gain (64×) the parts belonging to the trigonal $[Cr_{Ga}^+(A^{2-})$-$S_P^{6+}(A^+)]$ pair are marked by arrows. The numbers 1× and 64× indicate the multiplication factor of a normalized gain.

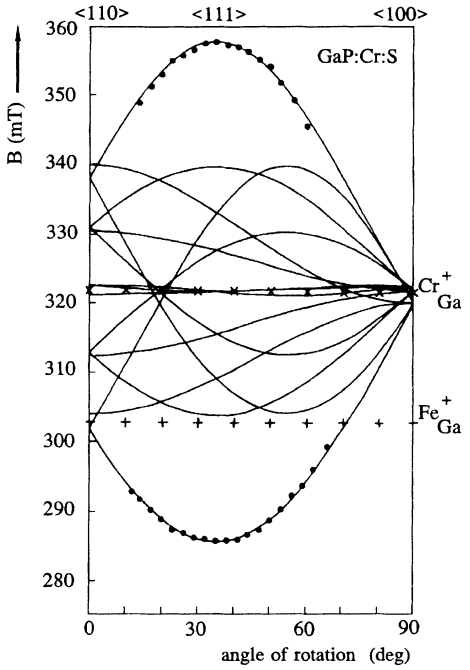

FIG. 5. Angular dependence of the fine structure of the trigonal $[Cr_{Ga}^+(A^{2-})$-$S_P^{6+}(A^+)]$ pair at 9.01 GHz. The magnetic field is rotated in a {110} plane. The experimental data are given for the trigonal pair by solid circles. The experimental line positions for the isolated defects $Cr_{Ga}^+(A^{2-})$ and $Fe^+(A^{2-})$ are also included and marked by × and +, respectively. The calculated angular dependence of the fine structure for the trigonal pair is plotted as solid lines for the transitions $\Delta M=\pm 1$. The used parameters are given in Table I.

iron-sulfur pair defect. In the present case the energy matrix of the spin Hamiltonian can be solved by perturbation theory in the weak-crystal-field limit with a sufficient accuracy. The allowed ($\Delta M=\pm 1$) electronic spin transitions are plotted in Fig. 5 by solid lines. The parameters of the best fit are given in Table I. But it should be noted that the analysis of the few experimental points given in Fig. 5 does not provide unique proof of the assumed spin value of $S=\frac{5}{2}$. The small part of the angular dependence which alone can be observed experimentally on account of the superposition with other stronger signals can also be fitted with other spin values. Arguments for the pair model including Cr_{Ga}^+ with $S=\frac{5}{2}$ are as follows.

(i) The Fermi level E_F in the samples is at or above the Cr_{Ga}^+/Cr_{Ga}^{2+} level so that most of the Cr_{Ga} are in the Cr_{Ga}^+ state.

(ii) The trigonal zero-field parameter D is expected to be much larger for the other possible charge states Cr_{Ga}^{2+} and Cr_{Ga}^{3+} which have no S-like orbital singlet ground states. Compare the D values of the possible Cr^{3+} complex in GaP (Ref. 17) (the D value was not determined but the spectrum could be described in the $S'=\frac{1}{2}$ formalism which is only valid for $D\gg g\mu_B B$) of the Cr_{Ga}^{3+}-Zn pair in Sec. III B as well as of the Jahn-Teller ions Cr_{Ga}^{2+} in GaAs,[18] Cr_{In}^{2+} in InP,[19] and Cr_{Ga}^{3+} in GaAs (Ref. 20) and GaP.[21]

According to our model of the $[Cr^{+}_{Ga}(A^{2-})\text{-}S^{6+}_{P}(A^{+})]$ pair the measured EPR lines were assigned to the spin transitions from $M=\pm\frac{5}{2}$ to $M'=\pm\frac{3}{2}$. As we were not able to observe other transitions, it was not possible to determine the parameters a and F. But we can expect that their contributions to the EPR line positions are small. The value of a for the Cr^{+} ion in the II-VI materials is in the order of 5×10^{-4} cm^{-1}.[22] In this case we were not able to determine the sign of D via the measurement of the temperature dependence of the line intensities since the spectrum is strongly saturated at temperatures below 20 K. The concentration of the $[Cr^{+}_{Ga}(A^{2-})\text{-}S^{6+}_{P}(A^{+})]$ pair was estimated from the spectra to be about 1% of the concentration of the isolated $Cr^{+}_{Ga}(A^{2-})$ centers.

B. GaP:Cr:Zn and GaP:Fe:Zn

In the p-type GaP samples codoped with Cr and Zn the known intense signal due to $Cr^{4+}_{Ga}(A^{+})$ (Ref. 23) is measured ($\Delta B_{pp}=8.5$ mT) as well as the $Fe^{3+}_{Ga}(A^{0})$ signal of residual iron (see Fig. 6). The occurrence of the Cr^{4+}_{Ga} charge state with a $^3A_2$ ground state was proved by an EPR experiment under uniaxial stress as it was done for Cr^{4+}_{Ga} in GaAs.[24] In dependence on the strength of the applied uniaxial stress a splitting into two lines could be observed confirming the spin value $S=1$. The EPR spectra of Cr^{4+}_{Ga} without and under uniaxial stress are shown in Fig. 7. Additionally, a strongly angular-dependent spectrum consisting of many lines is measured in the temperature range between 4 and 30 K. The spectra measured for the two main directions $\mathbf{B}\|\langle110\rangle$ and $\langle100\rangle$ are shown in Fig. 6 where the lines of the spectrum are marked by arrows. The measured angular dependence of the lines is plotted as solid circles in Fig. 8(b). Obviously, the center responsible for this spectrum has low symmetry.

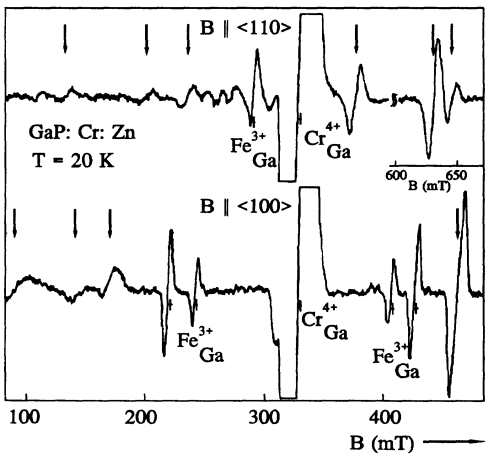

FIG. 6. EPR spectra of GaP:Cr:Zn measured at $T=20$ K with the microwave frequency of 9.008 GHz for the two main direction $\mathbf{B}\|\langle110\rangle$ and $\langle100\rangle$. The transitions belonging to the monoclinic $[Cr^{3+}_{Ga}(A^{0})\text{-}Zn^{2+}_{Ga}(A^{-})]$ pair are marked by arrows. Besides the pair spectrum the transitions originating from the isolated $Cr^{4+}_{Ga}(A^{+})$ and the residual $Fe^{3+}_{Ga}(A^{0})$ can be seen.

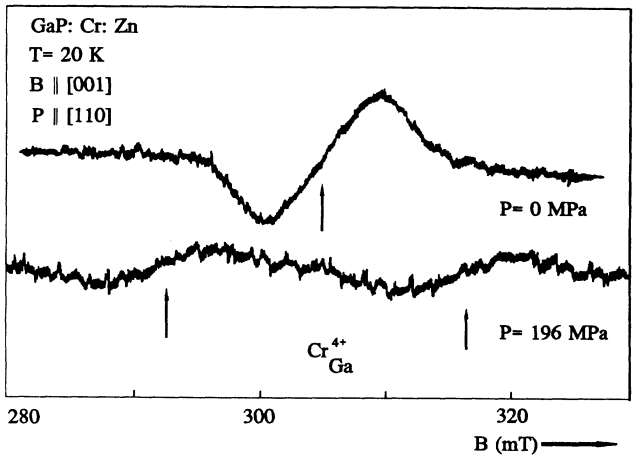

FIG. 7. Influence of $\langle110\rangle$ uniaxial stress on the EPR spectrum of the isolated Cr_{Ga} center in GaP:Cr:Zn. The splitting into two lines under stress proves the Cr^{4+}_{Ga} charge state with the spin $S=1$. Background signals were subtracted.

As in the cases reported in Sec. III A, the arguments of the chromium doping and the linewidth of the signals suggest that we observe a chromium-related defect. The subsequent analysis will show that the spectrum is caused by a $Cr^{3+}_{Ga}(A^{0})$ ion in monoclinic symmetry. A monoclinic distortion of a tetrahedral crystal field splits the ^4F ground state of the free Cr^{3+} ion and the lowest level is a $^4A_2$ orbital singlet state arising from the $^4T_1$ ground state in tetrahedral symmetry. Reasonably assuming a symme-

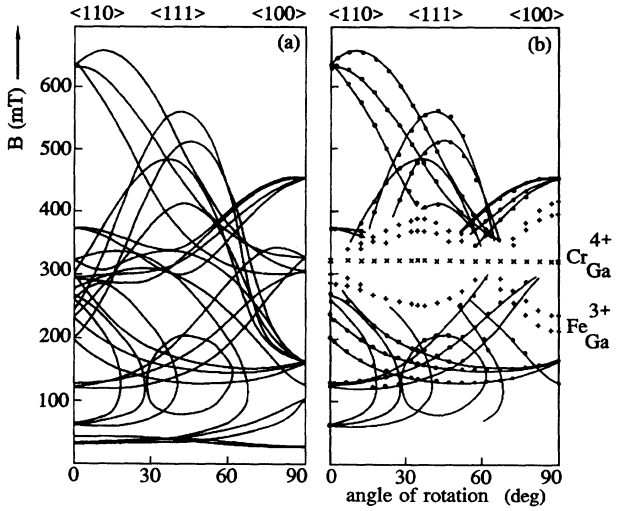

FIG. 8. Angular dependence of the fine-structure line positions of GaP:Cr:Zn at 9.008 GHz. The magnetic field is rotated in a {110} plane. (a) All calculated fine-structure transitions for the monoclinic $[Cr^{3+}_{Ga}(A^{0})\text{-}Zn^{2+}_{Ga}(A^{-})]$ pair. The parameters are given in Table I. (b) The experimental data for the monoclinic pair are given by solid circles. In order to compare with (a), those parts of the calculated angular dependence for which experimental data exist are indicated by solid lines. The other observed transitions belonging to the $Cr^{4+}_{Ga}(A^{+})$ and $Fe^{3+}_{Ga}(A^{0})$ isolated defects are marked by $\times$ and $+$, respectively.

trical g matrix, the spin Hamiltonian

$$\mathcal{H}=\mu_B \sum_{j,i} B_j g_{ji} S_i + S_j D_{ji} S_i \quad (2)$$

is used for the analysis, where j,i label the components within the chosen crystal axes $\mathbf{z},\mathbf{x}\|\langle 110\rangle$ and $\mathbf{y}\|\langle 100\rangle$. The magnitude of the experimental splitting of the electronic spin transitions (see Fig. 8) shows that we have to deal with an intermediate case, where the energy of the zero-field splitting has the same order of magnitude as the microwave energy in the X band. Therefore an analysis for all transitions using perturbation theory is not adequate for this system.

In order to proceed we have applied the method of direct computer diagonalization of the spin Hamiltonian (2) for fitting the experimental angular dependence of the electronic spin transitions. In Fig. 8(a) the results of the calculations are shown for all possible EPR transitions. In Fig 8(b) the calculated curves for which experimental data exist are included as solid lines to demonstrate the good agreement between theory and experiment. The best fit is achieved with the data given in Table I. The tensor axes x,y,z (given above) were chosen in such a way that D_{zz} is the largest component. The nondiagonal element D_{zy}, disappears if one makes a transformation into the principal axes by a rotation around the x axis. The rotation angle was determined to be about 10°. $D=-0.158$ cm^{-1} and $E=0.045$ cm^{-1} are the principal values using the common substitution $D=\frac{3}{2}D_{zz}$ and $E=\frac{1}{2}(D_{xx}-D_{yy})$. It should be pointed out that besides the determination of the spin value and the parameters of the spin Hamiltonian, also the monoclinic symmetry of the center was confirmed by the fit. In monoclinic symmetry the number of magnetically different center positions is reduced from 24, the maximum number of different center positions in a cubic crystal system, to 12. In our case the only symmetry element is a $\{110\}$ mirror plane. If the magnetic field is rotated around a $\langle 110\rangle$ axis, as it was done in our experiment, the number of magnetically nonequivalent centers is further reduced to 7. For the two main directions $\mathbf{B}\|\langle 110\rangle$ and $\langle 100\rangle$ the energy-level structure for an $S=\frac{3}{2}$ ground-state multiplet in dependence on the magnetic field has been deduced from the calculation of the energy matrix and is plotted in Figs. 9 and 10. The possible EPR transitions in the X band are marked. In Figs. 9 and 10 the designation M_j with $j=1$ to 7 describes the seven different center positions, which degenerate for the main directions $\mathbf{B}\|\langle 110\rangle$ and $\langle 100\rangle$ into four or two magnetically nonequivalent positions of the center, respectively. The lines belonging to the positions M_2 and M_3 are single lines, whereas all others are double ones.

From an analysis of the line positions as described above, it is only possible to determine the absolute value and relative signs of the tensor elements D_{ij}. A simultaneous change of the signs of D_{ij} produces an inversion of the sequence of the energy levels. The method to determine the signs of D_{ij} is to compare theoretical and experimental line intensities at different temperatures, including the effect of the Boltzmann population. In this case we have compared the high-field lines of M_1 and $M_{2/3}$ for $\mathbf{B}\|\langle 110\rangle$, which are separated by about 1 cm^{-1} (see Fig. 9). Only the signs of the parameters used in Fig. 9 and given in Table I satisfy the temperature dependence of the intensities measured between 4 and 30 K.

The monoclinic distortion of the tetrahedral symmetry can only be caused by an associated defect. A Zn acceptor placed on a nearest-neighbor Ga site is most probable (see Sec. IV). Therefore, the center is named $[Cr_{Ga}^{3+}(A^0)$-$Zn_{Ga}^{2}(A^-)]$. There are two arguments ruling out an interpretation of the observed spectrum as being due to isolated Cr_{Ga}^{3+} in low symmetry stabilized by strains. First, the behavior of the temperature dependence of this spectrum is quite different from that of isolated Cr_{Ga}^{3+} in GaAs, and second, the symmetry differs from the observed orthorhombic one in the case of Cr_{Ga}^{3+} in GaAs.[20] It should be noted that the spectrum investigated here is completely different from the orthorhombic Cr^{3+} spectrum found in p-type GaP:Cr.[17] The concentration of the monoclinic pairs was experimentally estimated to be about 10% of the concentration of the isolated $Cr_{Ga}^{4+}(A^+)$ defects.

In p-type GaP:Fe:Zn samples only the EPR spectrum due to isolated $Fe_{Ga}^{3+}(A^0)$ was measured both in the dark and under illumination of the sample with light, i.e., no

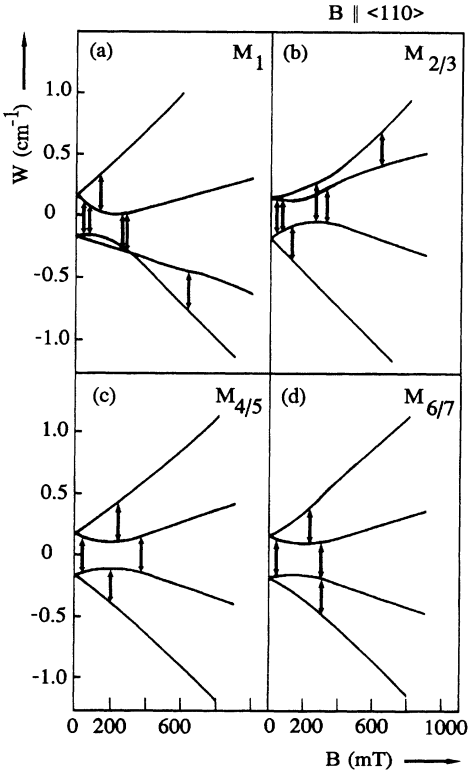

FIG. 9. Energy-level diagrams for the monoclinic $[Cr_{Ga}^{3+}(A^0)$-$Zn_{Ga}^{2+}(A^-)]$ pair for $\mathbf{B}\|\langle 110\rangle$. The designation M_j with $j=1$ to 7 describes the seven magnetically nonequivalent monoclinic center positions for the rotation in a $\{110\}$ plane. For the $\langle 110\rangle$ direction only four center positions are magnetically nonequivalent. Possible EPR transitions at 9.008 GHz are indicated by arrows.

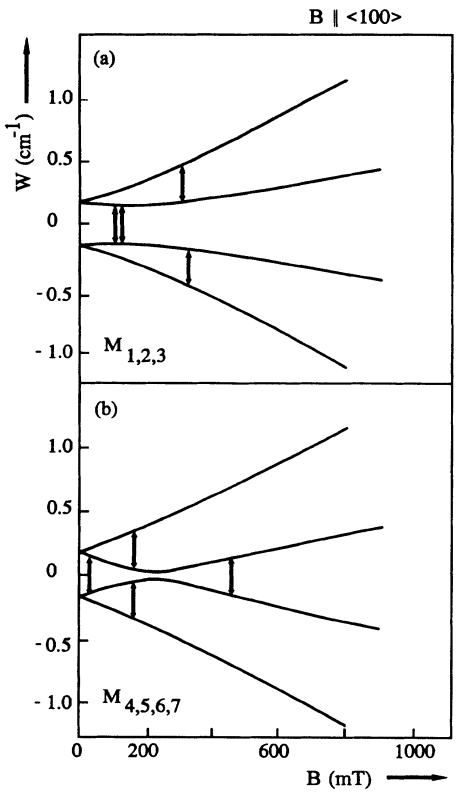

FIG. 10. Energy-level diagrams for the monoclinic $[Cr_{Ga}^{3+}(A^0)\text{-}Zn_{Ga}^{2+}(A^-)]$ pair for $\mathbf{B}\|\langle 100\rangle$. The designation M_j with $j=1$ to 7 describes the seven magnetically nonequivalent center positions for a rotation in a $\{110\}$ plane. For the $\langle 100\rangle$ direction only two magnetically nonequivalent center positions exist. Possible EPR transitions at 9.008 GHz are indicated by arrows.

spectrum attributable to an Fe-related complex could be detected.

IV. DISCUSSION

From the experimental results concerning symmetry and temperature dependence it was concluded that the three analyzed EPR spectra observed in the GaP samples are caused by complexes. The general problem for EPR investigations of TM-related defects in III-V semiconductors is the large linewidth caused by the interaction with the nuclear spins of the lattice constituents. This prevents the observation of a hyperfine structure also in the EPR spectra of the three TM complexes investigated in this paper. Therefore, unique proof of the chemical nature of the participating elements cannot be given. It is well known that the hyperfine interaction is the best tool for such an identification. But the following discussion will give several arguments supporting our assignment of the observed spectra to the proposed models without contradiction to the accepted results of the behavior of TM, shallow group-IIB acceptors, and group-VI donors in III-V materials.

In both *n*-type materials, GaP:Cr:S and GaP:Fe:S, a trigonal defect was observed. The linewidths of the trigonal defect spectra are of the same magnitude as those of the corresponding isolated Fe_{Ga}^{+} and Cr_{Ga}^{+}, which are the dominating defects in the materials. These facts suggest that the trigonal defects contain the TM. From the angular dependence of the fine-structure lines of GaP:Fe:S it was derived that the spectrum is caused by an $Fe_{Ga}^{+}(A^{2-})$ center ($3d^7$) in a cubic crystal field ($^4A_2$ ground state) with a considerable trigonal distortion. The observed g shift is characteristic for a $3d^7$ ion. The angular dependence of the observable fine-structure lines of GaP:Cr:S was interpreted as being due to a Cr_{Ga}^{+} center ($3d^5$) with a $^6S_{5/2}$ ground state in a trigonally distorted cubic crystal field as well.

In both cases the trigonal distortion suggests an associated defect on a nearest-neighbor phosphorus site. The main arguments for an associated S ion are the high content of S in the samples ($4\text{–}7\times10^{17}$ cm^{-3}) and the absence of the trigonal spectra in GaP:Fe and GaP:Cr samples without S doping. It is known that S on a substitutional phosphorus site acts as a shallow donor. The oxidation state of the S ion is most probably $S_P^{6+}(A^+)$ since the influence on the electronic structure of the complex is mainly to produce a trigonal crystal-field distortion. This behavior is characteristic of a closed-shell ion. The sixfold positive charge state based on a rather simple model building up the predominant covalent GaP lattice from $Ga^{3+}P^{5+}$ residual ions completed with eight binding electrons. In this picture the residual ion of the S donor has to be described as $S_P^{5+}(A^0)/S_P^{6+}(A^+)$. The residual ions give rise to the EPR spectra, usually. If the more ionic description of the crystal, $Ga^{3+}P^{3-}$, is used the same S donor states can be characterized by $S_P^{3-}(A^0)/S_P^{2-}(A^+)$. The position of the TM-S pairs $[Fe_{Ga}^{+}(A^{2-})\text{-}S_P^{6+}(A^+)]$ and $[Cr_{Ga}^{+}(A^{2-})\text{-}S_P^{6+}(A^+)]$ in the lattice is shown in Fig. 11. The line between the constituents of the complex is oriented along a $\langle 111\rangle$ direction.

In the *p*-type GaP:Cr:Zn samples we observed a monoclinic defect. As in the case of the two trigonal centers discussed above, the Cr doping and the observed

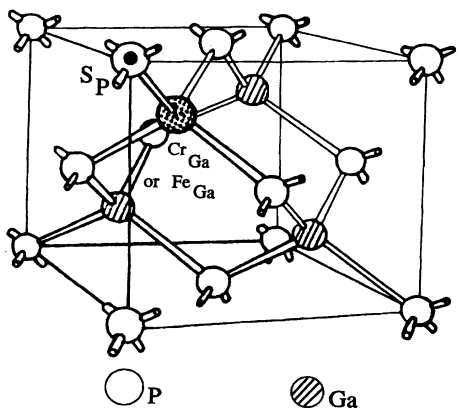

FIG. 11. Structural model for the $[T_{Ga}^{+}(A^{2-})\text{-}S_P^{6+}(A^+)]$ pair center in *n*-type GaP with T=Fe or Cr (where T denotes the transition metal).

linewidth suggest a Cr-related defect. The isolated charged donor state $Cr_{Ga}^{4+}(A^+)$ is the dominating defect in the samples. The angular dependence of the fine-structure lines of the spectrum shows the general feature of a $Cr_{Ga}^{3+}(A^0)$ ion ($3d^3$) in a monoclinic distorted cubic crystal field with a $^4A_2$ orbital singlet as the ground state. All the details of the observed fine structure can be understood as being due to transitions within this $S=\frac{3}{2}$ ground state manifold.

As a Jahn-Teller distortion can be ruled out, the observed low symmetry of the $Cr_{Ga}^{3+}(A^0)$ containing center must be created by an associated defect. The monoclinic symmetry of the complex defect can be explained by the pairing of Cr_{Ga} with Zn_{Ga} on a nearest-neighbor Ga site. That Zn_{Ga} is the associated defect is strongly suggested by the high Zn concentration (5×10^{17} cm^{-3}) and by the result that the monoclinic spectrum was not detected in GaP:Cr material without additional Zn doping. The position of the $[Cr_{Ga}^{3+}(A^0)\text{-}Zn_{Ga}^{2+}(A^-)]$ pair in the GaP lattice is shown in Fig. 12. The tensor axes used for the EPR analysis and the mirror plane of the monoclinic symmetry are included. The line between the two constituents of the pair is oriented along a $\langle 110\rangle$ direction. It is evident from Fig. 12 that the particular P atom connecting the Cr and Zn ions is nonequivalent with the other three P atoms surrounding the Cr_{Ga}. This Cr_{Ga}-P-Zn_{Ga} triangle determines the $\{110\}$ mirror plane.

During the pairing the charge state of the Cr_{Ga} is converted from the charged donor state $Cr_{Ga}^{4+}(A^+)$ (the state of the isolated Cr_{Ga} centers) to the neutral $Cr_{Ga}^{3+}(A^0)$ state within the pair. That means that the energy level of the pair $[Cr\text{-}Zn]^{0/-}$ must be located below the level of the isolated $Cr_{Ga}^{3+}/Cr_{Ga}^{4+}$ and also below the Fermi level pinned in our samples by the Zn_{Ga} acceptors.

The concentrations of all three pair defects are in the range between 1% and 10% of the concentration of the isolated TM defects. Assuming a statistical distribution of the TM ions and shallow defects using their measured concentrations one would expect only a nearest-neighbor concentration of about 0.1%.[25] For the high concentration of pairs two reasons can be responsible. First, there exists an attractive force between the constituents of the pair stimulating the formation, and second, the distribution of the isolated defects is strongly inhomogeneous in different macroscopic parts of the samples. The second reason is very unlikely in LEC-grown material as it supposes that the defect concentration fluctuates by several orders of magnitude. Therefore, for the formation of the TM shallow defect pairs a donor-acceptor pairing mechanism is responsible driven by the Coulomb attraction between the constituents. In the case of the *n*-type GaP the pair consists of a double negatively charged TM acceptor (Cr^+ or Fe^+) and a positively charged shallow donor (S_P). On the other hand, in *p*-type GaP the TM (Cr_{Ga}) acts as a positively charged deep donor associated with a negatively charged shallow acceptor (Zn_{Ga}).

We failed in the attempt to observe an analogous Fe-Zn pair in *p*-type GaP:Fe:Zn although the doping concentrations are nearly the same as in GaP:Cr:Zn. The reason might be that Fe_{Ga} does not form a donor level $Fe_{Ga}^{3+}/Fe_{Ga}^{4+}$ within the gap of GaP [in *p*-conducting GaP:Fe:Zn all isolated iron is in the $Fe_{Ga}^{3+}(A^0)$ charge state]. This result supports the Coulomb mechanism for the donor-acceptor pair formation, which requires the existence of the charged donor state $T_{Ga}^{4+}(A^+)$ for the pairing with a shallow acceptor.

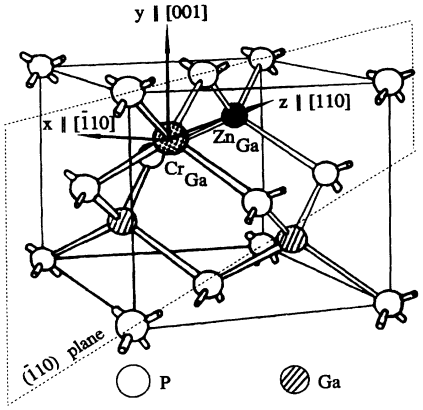

FIG. 12. Structural model for the $[Cr_{Ga}^{3+}(A^0)\text{-}Zn_{Ga}^{2+}(A^-)]$ pair center in *p*-type GaP. The $(\bar{1}10)$ mirror plane and the tensor axes used for the EPR analysis are included.

V. CONCLUSIONS

The analysis of the EPR spectra of LEC-grown GaP:Cr:S, GaP:Fe:S, and GaP:Cr:Zn has evidenced three donor-acceptor pair centers. The $[Fe_{Ga}^{+}(A^{2-})\text{-}S_P^{6+}(A^+)]$ pair of trigonal symmetry is the first identified Fe-related pair defect in as-grown III-V semiconductors. With the $[Cr_{Ga}^{3+}(A^0)\text{-}Zn^{2+}(A^-)]$ pair of monoclinic symmetry a pair defect is found for the first time where the transition metal (T_{Ga}) acting as a deep donor complexed with a shallow acceptor (Zn_{Ga}). Together with the $[Cr_{Ga}^{+}(A^{2-})\text{-}S_P^{6+}(A^+)]$ pair this demonstrates the existence of donor-acceptor pairs in III-V semiconductors with a T_{Ga} acting alternatively as double acceptor (Cr_{Ga}^{+}/Cr_{Ga}^{2+}) or as donor ($Cr_{Ga}^{3+}/Cr_{Ga}^{4+}$). The concentration of these pair defects amounts to about 1–10 % of the isolated T_{Ga} and is, therefore, within the same concentration range as the Ni_{Ga}^{+} shallow donor pairs found in GaAs and GaP.[3] This strongly suggests that Coulomb attraction is responsible for the formation of T_{Ga} shallow impurity pairs in III-V semiconductors.

ACKNOWLEDGMENTS

The authors would like to thank K. Irmscher for his useful comments and I. Gründler for technical assistance.

[1]B. Clerjaud, J. Phys. C **18**, 3615 (1985).
[2]A. Zunger, in *Solid State Physics,* edited by H. Ehrenreich, F. Seitz, and D. Turnbull (Academic, New York, 1986), Vol. 39, p. 275.
[3]H. Ennen, U. Kaufmann, and J. Schneider, Appl. Phys. Lett. **38**, 355 (1981).
[4]G. G. P. van Gorkom and A. T. Vink, Solid State Commun. **11**, 767 (1972).
[5]B. Deveaud, B. Lambert, P. Auvray, A. M. Hennel, B. Clerjaud, and C. Naud, J. Phys. C **19**, 1251 (1986).
[6]B. Deveaud, B. Lambert, G. Picoli, and G. Martinez, J. Appl. Phys. **55**, 4356 (1984).
[7]J. A. L. Simpson, C. A. Bates, J. Barrau, M. Brousseau, and V. Thomas, Semicond. Sci. Technol. **3**, 178 (1988).
[8]A. Kana-ah, B. C. Cavenett, B. Monemar, and H P. Gislason, Semicond. Sci. Technol. **2**, 151 (1987).
[9]H. P. Gislason, B. Monemar, and P. Bergman, Phys. Rev. B **38**, 5466 (1988).
[10]R. S. Title, J. Appl. Phys. **40**, 4902 (1969).
[11]W. Gehlhoff, K. Irmscher, and J. Kreissl, in *New Developments in Semiconductor Physics,* edited by G. Ferenczi and F. Beleznay, Lecture Notes in Physics Vol. 301 (Springer-Verlag, Berlin, 1988), p. 262; J. Kreissl, W. Gehlhoff, P. Omling, and P. Emanuelsson, Phys. Rev. B **42**, 1731 (1990).
[12]J. Kreissl, W. Ulrici, U. Rehse, and W. Gehlhoff, in *Proceedings of the 20th International Conference of the Physics of Semiconductors,* edited by E. M. Anastassakis and J. D. Joannopoulos (World Scientific, Singapore, 1990), p. 682.
[13]U. Kaufmann and J. Schneider, Solid State Commun. **21**, 1073 (1977).
[14]A. Abragam and B. Bleaney, *Electron Paramagnetic Resonance of Transition Ions* (Clarendon, Oxford, 1970).
[15]S. Brehme and R. Pickenhain, Physica **145B**, 267 (1987).
[16]U. Kaufmann and W. H. Koschel, Phys. Rev. B **17**, 2081 (1978).
[17]U. Kaufmann and J. Schneider, Adv. Electron. Electron Phys. **58**, 81 (1982).
[18]J. J. Krebs and G. H. Stauss, Phys. Rev. B **16**, 971 (1977); C. A. Bates, M. Darcha, J. Handley, A. Vasson, and A.-M. Vasson, Semicond. Sci. Technol. **3**, 172 (1988).
[19]J. Handley, C. A. Bates, A. Vasson, A.-M. Vasson, K. Ferdjani, and N. Tebbal, Semicond. Sci. Technol. **5**, 710 (1990).
[20]J. J. Krebs and G. H. Stauss, Phys. Rev. B **15**, 17 (1977); L. W. Parker, C. A. Bates, J. L. Dunn, A. Vasson, and A.-M. Vasson, J. Phys. Condens. Matter **2**, 2481 (1990).
[21]M. Darcha, A. Vasson, A.-M. Vasson, C. A. Bates, and J. L. Dunn, J. Phys. C **20**, 2261 (1987).
[22]R. S. Title, in *Physics and Chemistry of II-VI Compounds,* edited by M. Aven and J. S. Prener (North-Holland, Amsterdam, 1967).
[23]U. Kaufmann and J. Schneider, Appl. Phys. Lett. **36**, 747 (1980).
[24]J. J. Krebs and G. H. Stauss, Phys. Rev. B **26**, 2296 (1982).
[25]U. W. Pohl and W. Busse, J. Chem. Phys. **90**, 6877 (1989).